Endoplasmic reticulum calnexins participate in the primary root growth response to phosphate deficiency

Jonatan Montpetit[a,2], Joaquín Clúa[a,2], Yi-Fang Hsieh[a], Evangelia Vogiatzaki[a], Jens Müller [b], Steffen Abel [b], Richard Strasser [c], Yves Poirier [a, 3, 4]

[a] Department of Plant Molecular Biology, Biophore Building, University of Lausanne, 1015 Lausanne, Switzerland

[b] Department of Molecular Signal Processing, Leibniz Institute of Plant Biochemistry, 06120 Halle, Germany

[c] Department of Applied Genetics and Cell Biology, University of Natural Resources and Life Sciences, Vienna, Muthgasse 18, A-1190 Vienna, Austria

Short title: Calnexin and phosphate deficiency

One sentence summary: Calnexin, a lectin chaperone engaged in the folding of N-glycosylated proteins in the endoplasmic reticulum, participates in primary root adaptation to low phosphate conditions.

Footnotes

[2] These authors have contributed equally to this work.

[3] Corresponding Author: Yves.Poirier@unil.ch

[4] Senior author

The author responsible for distribution of materials integral to the findings presented in this article in accordance with the policy described in the Instruction for Authors (https://academic.oup.com/plphys/pages/General-Instructions) is: Yves Poirier (yves.poirier@unil.ch).

Author Contributions

J Montpetit and YP conceived the project. J Montpetit and JC contributed equally to all experiments, with the exception of GUS and GFP analysis, which was performed by EV and YFH, respectively. J Müller and SA helped with the analysis of Fe deposition, and RS helped generate several plant lines. YP and JC wrote the manuscript. All authors read and approved the final manuscript. YP agrees to serve as the author responsible for contact and ensures communication.

Abstract

Accumulation of incompletely folded proteins in the endoplasmic reticulum (ER) leads to ER stress, activates ER protein degradation pathways, and upregulates genes involved in protein folding. This process is known as the unfolded protein response (UPR). The role of ER protein folding in plant responses to nutrient deficiencies is unclear. We analyzed Arabidopsis (*Arabidopsis thaliana*) mutants affected in ER protein quality control and established that both *CALNEXIN* (*CNX*) genes function in the primary root response to phosphate (Pi) deficiency. CNX1 and CNX2 are homologous ER lectins promoting protein folding of N-glycosylated proteins via the recognition of the $GlcMan_9GlcNAc_2$ glycan. Growth of *cnx1-1* and *cnx2-2* single mutants was similar to that of the wild type under high and low Pi conditions, but the *cnx1-1 cnx2-2* double mutant showed decreased primary root growth under low Pi conditions due to reduced meristematic cell division. This phenotype was specific to Pi deficiency; the double mutant responded normally to osmotic and salt stress. Expression of CNX2 mutated in amino acids involved in binding the $GlcMan_9GlcNAc_2$ glycan failed to complement the *cnx1-1 cnx2-2* mutant. The root growth phenotype was Fe dependent and was associated with root apoplastic Fe accumulation. Two genes involved in Fe-dependent inhibition of primary root growth under Pi deficiency, the ferroxidase *LOW PHOSPHATE 1 (LPR1*) and P5-type ATPase *PLEIOTROPIC DRUG RESISTANCE 2* (*PDR2*) were epistatic to *CNX1/CNX2*. Overexpressing *PDR2* failed to complement the *cnx1-1 cnx2-2* root phenotype. The *cnx1-1 cnx2-2* mutant showed no evidence of UPR activation, indicating a limited effect on ER protein folding. CNX might process a set of N-glycosylated proteins specifically involved in the response to Pi deficiency.

Introduction

The endoplasmic reticulum (ER) serves as the major entry point for proteins into the secretory pathway as well as for proteins destined for the plasma membrane (PM). It is estimated that approximately one-third of cellular proteins pass through this organelle (Strasser, 2018). The ER is thus a major site for folding and quality control of proteins involved in numerous cellular processes, including cell wall synthesis, nutrient transport, and PM-based signal transduction (Brandizzi, 2021). The ER harbors two main pathways to assist in protein folding. The first pathway involves the general chaperones BINDING PROTEINS (BiPs), which belong to the classical heat shock protein 70 (HSP70) family, the DNA J protein ERdj3 and its associated STROMAL-DERIVED FACTOR 2 (SDF2) protein, and protein disulfide isomerases (PDI), which promote the formation of disulfide bonds (Strasser, 2018). The second pathway, a distinct ER folding pathway known as the calnexin-calreticulin cycle, is dedicated to N-glycosylated proteins. Calnexin and calreticulin are lectins that share a common architecture consisting of two major domains: a glycan binding domain and a long flexible P-domain involved in recruiting other co-chaperones such as PDIs. While calnexin is anchored to the ER via a transmembrane domain, its homologue calreticulin is soluble within the ER matrix and harbors a luminal KDEL ER retrieval signal (Strasser, 2018; Kozlov and Gehring, 2020). Arabidopsis (*Arabidopsis thaliana*) contains two *CALNEXIN* (*CNX*) genes and three *CALRETICULIN* (*CRT*) genes (Persson et al., 2003; Liu et al., 2017).

In the CNX-CRT cycle, proteins entering the ER are first conjugated with a $Glc_3Man_9GlcNAc_2$ glycan on specific asparagines (ASN) by the oligosaccharyltransferase (OST) complex. The N-linked glycans are then trimmed by two glucosidases (GCSI and GCSII) to generate a monoglucosylated $GlcMan_9GlcNAc_2$ glycan, which specifically interacts with CNX or CRT to promote protein folding and maturation. Removal of the terminal glucose by GCSII leads to the release of the glycoprotein from CNX/CRT. If the protein is inappropriately folded after release, the glucosyltransferase UDP-glucose:glycoprotein glucosyltransferase (UGGT) adds back a terminal glucose, enabling the re-association of the misfolded glycoprotein with CNX or CRT and thus initiating an additional round of folding (Liu and Howell, 2010; Strasser, 2018).

ER proteins that repeatedly fail to properly fold after several rounds of the CNX-CRT cycle are directed to become degraded. An important pathway for ER protein degradation involves the

translocation of misfolded proteins to the cytosol for proteasomal degradation, a process termed ER-associated degradation (ERAD). Protein degradation through ERAD involves the recognition and transport of misfolded proteins across the ER membrane to the cytosol, followed by polyubiquitination and degradation via the 26S proteasome (Chen et al., 2020). The accumulation of misfolded proteins in the ER leads to ER stress and the activation of the unfolded protein response (UPR). In turn, the activation of the UPR results in the upregulation of genes involved in vesicular trafficking, ERAD, and protein folding, including *BiPs* and *PDIs* (Liu and Howell, 2016). The UPR signaling pathway has two branches. In the first branch, the ER-anchored RNA splicing factor INOSITOL-REQUIRING 1 (IRE1) modifies the mRNA of the transcription factor BASIC LEUCINE-ZIPPER 60 (bZIP60), yielding a form of bZIP60 that lacks a transmembrane domain and is targeted to the nucleus. The second branch of the UPR signaling pathway activates two other members of the bZIP family, bZIP17 and bZIP28, via protease processing in the Golgi (Liu and Howell, 2016). Chronic ER stress that cannot be resolved by the activation of ERAD and the UPR can lead to programmed cell death as well as autophagy (Manghwar and Li, 2022).

ER stress has been associated with numerous abiotic stress factors that are thought to lead to defects in protein folding in the ER, such as heat, drought, osmotic, salt, and metal stress. The link between the control of ER protein folding and abiotic stress has been demonstrated via the analysis of mutants as well as transgenic plants overexpressing genes encoding ER chaperones, such as *BiP*, *CNX*, and *PDIs*, as well as genes involved in the ERAD and UPR pathways, including *INOSITOL-REQUIRING 1* (*IRE1)* and *bZIP28* (Gao et al., 2008; Deng et al., 2011; Kim et al., 2013; Joshi et al., 2019; Park and Park, 2019; Reyes-Impellizzeri and Moreno, 2021). However, whether the control of protein folding in the ER has a role in plant responses to nutrient deficiencies has not been determined, although recent work has shown that autophagy may be implicated in such stress (Naumann et al., 2019; Stephani et al., 2020; Yoshitake et al., 2021).

Phosphorus is one of the most important nutrients affecting plant growth in both agricultural and natural ecosystems (Poirier et al., 2022). Plants acquire phosphorus almost exclusively via the transport of soluble inorganic phosphate ($H_2PO_4^-$; Pi) into roots. Plants have evolved a series of metabolic and developmental responses to Pi deficiency that are aimed at maximizing Pi acquisition from the environment and optimizing its internal use for growth and reproduction (Dissanayaka et al., 2021; Poirier et al., 2022). One of the best-characterized responses of roots

to phosphate deficiency is a decrease in primary root growth associated with reduced root meristem size (Crombez et al., 2019). This phenotype has been associated with the presence of Fe^{+3}-malate complexes in the root meristem leading to changes in the cell wall structure and inhibition of cell-to-cell communication (Müller et al., 2015; Balzergue et al., 2017; Mora-Macias et al., 2017). Genetic screens for genes that contribute to changes in primary root growth under Pi deficiency identified *LOW PHOSPHATE 1* (*LPR1)* and *LPR2*, encoding ferroxidases that convert Fe^{+2} to Fe^{+3}, and *PLEIOTROPIC DRUG RESISTANCE 2* (*PDR2*), encoding an ER-localized P5-type ATPase thought to negatively affect LPR activity via an unknown mechanism (Ticconi and Abel, 2004; Svistoonoff et al., 2007; Ticconi et al., 2009; Naumann et al., 2022). Additional proteins found to participate in this pathway include the malate and citrate efflux channel ALUMINUM-ACTIVATED MALATE TRANSPORTER 1 (ALMT1); the SENSITIVE TO PROTON RHIZOTOXICITY 1 (STOP1) transcription factor, which regulates *ALMT1* expression; ALUMINUM SENSITIVE 3 (ALS3) and SENSITIVE TO AL RHIZOTOXICITY 1 (STAR1), which together form a tonoplast ABC transporter complex involved in plant tolerance to aluminum (although the nature of the molecule that is transported remains to be defined); and the CLAVATA/ESR-RELATED 14 (CLE14) peptide receptors CLAVATA 2 (CLV2) and PEP1 RECEPTOR 2 (PEPR2) (Balzergue et al., 2017; Dong et al., 2017; Gutierrez-Alanis et al., 2017; Mora-Macias et al., 2017).

In the present study, we analyzed Arabidopsis mutants affected in components of ER protein folding and quality control for their response to phosphate deficiency. We determined that CNX proteins participate in the Fe-dependent inhibition of primary root growth in response to phosphate deficiency.

Results

The *cnx1 cnx2* double mutant shows reduced primary root growth under low Pi conditions

We crossed the Arabidopsis *cnx1-1* mutant (SALK_083600), which has a T-DNA insertion in the 3rd exon of *CNX1* (At5g61790), with *cnx2-2* (SAIL_865_F08) and *cnx2-3* (SAIL_580_H02), which have T-DNA insertions in the third exon of *CNX2* (At5g07340), to create two independent double mutant combinations (Figure 1A). Immunoblot analysis of protein extracts from whole seedlings showed that CNX proteins were absent in the *cnx1-1 cnx2-2* double mutant, indicating that these mutant alleles are likely null (Figure 1B). We grew the plants in fertilized soil and in clay irrigated with nutrient solution containing 1 mM Pi (high Pi; HPi) or 75 µM Pi (low Pi; LPi) and found no significant differences between the single and double mutants compared to the wild type (WT; Col-0) in terms of fresh weight (Supplemental Figure S1A, B) or Pi content in roots or rosettes (Supplemental Figure S1C). In agreement with these results, there was no significant difference in the amount of Pi acquired by the root system from liquid medium between the WT and the *cnx1-1 cnx2-2* double mutant, either on LPi and HPi conditions (Supplemental Figure S1D). By contrast, in seedlings grown on agar-solidified medium, primary root length was significantly reduced in the *cnx1-1 cnx2-2* and *cnx1-1 cnx2-3* double mutants compared to the WT under LPi but not HPi conditions (Figure 1C, E). This phenotype was complemented by transforming the *cnx1-1 cnx2-2* double mutant with the *CNX1-GFP* or *CNX2-GFP* fusion construct driven by their respective endogenous promoters (Figure 1D, E). Confocal microscopy of roots of the complemented lines expressing CNX1-GFP or CNX2-GFP revealed localization of these fusion proteins in the ER (Supplemental Figure S2A). Co-localization of CNX1-GFP and CNX2-GFP with an ER marker (ER-RFP) was observed in transiently transfected *Nicotiana benthamiana* leaf cells (Supplemental Figure S2B).

No difference in lateral root length was observed between the WT and the *cnx1-1 cnx2-2* double mutant for plants grown under LPi or HPi conditions (Figure 1F). However, an increase in lateral root density was observed in the *cnx1-1 cnx2-2* double mutant relative to the WT, but only under LPi (Figure 1G). Such an increase in lateral root density is likely associated to the decrease in primary root length observed in the *cnx1-1 cnx2-2* mutant under LPi.

Mutants in other components of the CNX/CRT cycle and ER chaperone system do not reproduce the *cnx1 cnx2* root growth phenotype under low Pi

In addition to CNX, ER protein quality control relies on numerous other proteins, including chaperones and enzymes involved in glycosylation and glycan modifications in the ER (Strasser, 2018). We therefore examined primary root growth of mutants in various components of the CNX/CRT cycle and ER protein quality control under LPi conditions. Arabidopsis CRTs are encoded by three genes, which are divided into two groups based on sequence similarity and function: *CRT1/CRT2* and *CRT3* (Persson et al., 2003; Christensen et al., 2010). No significant differences were detected in the root growth of *crt1 crt2* or *crt3* mutants under HPi or LPi conditions compared to WT (Figure 2A).

The synthesis of the lipid-linked oligosaccharide unit $Glc_3Man_9GlcNAc_2$ involves a series of ER glycosyltransferases including the mannosyltransferases ASPARAGINE-LINKED GLYCOSYLATION 3 (ALG3) and ALG9 and the glucosyltransferase ALG10 (Kajiura et al., 2010; Farid et al., 2011; Hong et al., 2012). Following its synthesis, the $Glc_3Man_9GlcNAc_2$ unit is added to ER proteins co-translationally by the membrane-associated heteromeric OST complex, which includes the catalytic STAUROSPORIN AND TEMPERATURE SENSITIVE 3 (STT3) subunit found as two isoforms in Arabidopsis, namely STT3a and STT3b (Koiwa et al., 2003). Primary root growth under HPi and LPi conditions was not reduced in the *alg3-1*, *alg9a*, *alg10-1*, or *stt3a2* mutants compared to WT (Figure 2A).

The presence of terminal α1,2-linked glucose residues, which facilitate the interaction between CNX/CRT and N-glycosylated proteins, is regulated by the trimming action of GCSII and the glucosylating activity of the UDP-glucose:glycoprotein glucosyltransferase (UGGT). *PRIORITY IN SWEET LIFE 5* (*PSL5)* and *PSL4* encode the alpha and beta subunits of GCSII, respectively, while the UGGT is encoded by a single *EBS1/UGGT* gene (Lu et al., 2009). The primary roots of the *psl4* mutant were shorter than those of WT when grown on HPi medium, and there was no significant further reduction in their length when grown on LPi medium (Figure 2A). In contrast, primary root growth was severely compromised in the *ebs1-6/uggt1-1* mutant on both HPi and low LPi media (Figure 2A).

ER proteins that pass through the CNX/CRT cycle but remain inappropriately folded are degraded by ERAD. This process involves the trimming of mannosyl groups on the N-glycan chain by several α-mannosidases, which include MANNOSIDASE 4 (MNS4) and MNS5 (Huttner et al., 2014). Primary root growth of the *mns4 mns5* double mutant was not significantly different from that of WT on HPi or LPi medium (Figure 2A).

We also examined the role of the ER chaperone pathway involving BiP and SDF2 in the response of Arabidopsis roots to Pi deficiency. While SDF2 is encoded by a single gene in Arabidopsis (Nekrasov et al., 2009), three genes encode the ER BiP chaperones. *BIP1* and *BIP2* encode proteins that are 99% identical and are ubiquitously expressed, while the more divergent *BiP3* is expressed under ER stress (Maruyama et al., 2014). Root growth of the *bip1-4 bip3-1*, *bip2-2 bip3-1*, and *sdf2-1* mutants was similar to that of WT on both HPi and LPi media (Figure 2B).

Several mutants related to the CNX/CRT cycle and ER protein homeostasis, including *alg10*, *stt3a*, *mns4 mns5*, and *ebs1-6*/*uggt1*, exhibit strong root growth phenotypes under salt stress (Koiwa et al., 2003; Farid et al., 2011; Huttner et al., 2014; Blanco-Herrera et al., 2015). To investigate whether the reduced primary root length observed in *cnx1-1 cnx2-2* was specific to Pi deficiency stress, we examined root growth in this double mutant under two other abiotic stress conditions that reduced primary root growth: osmotic stress (200 mM mannitol) and salt stress (100 mM NaCl). Under both stress conditions, primary root growth was similar in the *cnx1-1 cnx2-2* double mutant and WT (Figure 2C-D), indicating that the root growth phenotype of this double mutant is specific to Pi deficiency stress.

Complementation of the *cnx1 cnx2* root phenotype by CNX2 is dependent on amino acids involved in binding the $GlcMan_9GlcNAc_2$ glycan

Crystallographic analysis of mouse CRT combined with modeling as well as *in vitro* biochemical studies have identified a number of amino acids residues directly involved in binding the $GlcMan_9GlcNAc_2$ glycan (Kapoor et al., 2004; Thomson and Williams, 2005; Kozlov et al., 2010). Among them are Y109 and K111 which form hydrogen bonds with two distinct oxygens of the terminal glucose residue of $GlcMan_9GlcNAc_2$ (Kozlov et al., 2010). Mutation of the corresponding Y118 and K120 residues of the Arabidopsis CRT3 demonstrated the critical role, *in vivo*, of these amino acids in enabling the interaction of CRT3 with a structurally modified but active version of the BRI1 brassinosteroid receptor found in the *bri1-9* mutant (Liu and Li, 2013). Alignment of CNX2 with the Arabidopsis CRT3 and the mouse CRT enabled the identification of the corresponding Y122 and K124 residues in CNX2 (Figure 3A, Supplemental Figure S3). These two residues were independently mutated to alanine in a pCNX2::CNX2-GFP fusion construct and transformed into the *cnx1-1 cnx2-2* double mutant. While transformation with the WT pCNX2::CNX2-GFP enabled the complementation of the

cnx1-1 cnx2-2 short-root phenotype under LPi condition, neither the Y122A or K124A mutants could complement the *cnx1-1 cnx2-2* mutant root phenotype, although the mutant and WT constructs were all expressed in the ER of root tips (Figure 3B-C). These results reveal that the $GlcMan_9GlcNAc_2$ binding domain of CNX2 is critical for its role in maintaining primary root growth under LPi condition.

The root phenotype of *cnx1 cnx2* is due to reduced root apical meristem activity

Reduced primary root growth under stress conditions can be caused by reduced cell division within the meristem, reduced cell elongation, or both. Under LPi but not HPi conditions, the meristematic zone was smaller in *cnx1-1 cnx2-2* compared to WT and the corresponding single mutants (Figure 4A, B). By contrast, the cell length in the elongation zone was not significantly different between the mutants and WT under HPi or LPi conditions (Figure 4A, C). These data indicate that *cnx1-1 cnx2-2* is mainly affected in meristematic cell division under LPi conditions. To further evaluate the contribution of cell division to the mutant phenotype, we introduced into the *cnx1-1 cnx2-2* double mutant a reporter construct for cell division consisting of a labile GUS under the control of the cyclin B1 promoter (Colon-Carmona et al., 1999). The number of dividing, GUS-expressing cells, was similar in *cnx1-1 cnx2-2* and WT roots under HPi conditions (Figure 4D). By contrast, a clear reduction in GUS-expressing cells was observed in WT roots grown under LPi, in accordance with the known reduction in meristematic cell division under these conditions (Ticconi et al., 2004). Importantly, a further reduction in GUS-expressing cells in root meristems was observed in the *cnx1-1 cnx2-2* double mutant compared to WT on LPi (Figure 4D). Altogether, these data indicate that the altered primary root growth of *cnx1-1 cnx2-2* is primarily due to reduced meristematic cell division under LPi conditions.

The root phenotype of *cnx1-1 cnx2-2* is dependent on Fe and associated with increased Fe deposition in the meristem

Several studies have shown that the reduced primary root growth of plants under low Pi in WT and in various mutants with more severe root growth inhibition is dependent on the presence of Fe in the growth medium (Ticconi et al., 2009; Müller et al., 2015; Balzergue et al., 2017; Dong et al., 2017). Indeed, a comparison of root growth on HPi and LPi medium with and without Fe showed that the reduced primary root growth observed in *cnx1-1 cnx2-2* under LPi conditions was also dependent on the presence of Fe in the medium (Figure 2E-F). We used Perls-DAB staining to examine the distribution of apoplastic Fe in plants grown under HPi and LPi

conditions. The *lpr1* mutant (which is insensitive to low Pi-induced root growth inhibition) and *pdr2* mutant (which has very strongly reduced primary root growth under low Pi conditions) were used as controls (Müller et al., 2015). In plants grown under HPi conditions, no substantial differences were observed in Fe distribution in the root meristematic and elongation zones between WT and *cnx1-1 cnx2-2* or *pdr2*, whereas *lpr1* showed substantially reduced Fe deposition (Figure 5, upper panels). Under LPi conditions, the *cnx1-1 cnx2-2* double mutant showed robust enhancement of Fe deposition in the root differentiation zone and more modest enhancement in the root elongation and meristematic zones compared to WT, whereas *pdr2* roots showed extensive Fe deposition throughout the root, and *lpr1* showed minimal Fe deposition (Figure 5, lower panels).

pdr2 and _lpr1 lpr2_ are epistatic to _cnx1-1 cnx2-2_

We examined the epistasis among *cnx1-1 cnx2-2*, *lpr1 lpr2*, and *pdr2* by generating triple and quadruple mutants. Primary root growth of *cnx1-1 cnx2-2 lpr1 lpr2* was insensitive to low Pi, as the primary root length of this quadruple mutant was identical to that of *lpr1 lpr2* and longer than that of WT under LPi conditions (Figure 6A). The *pdr2* mutant showed reduced primary root growth in HPi; this phenotype remained unchanged in the *cnx1-1 cnx2-2 pdr2* triple mutant. On LPi medium, the *pdr2* mutant showed more strongly reduced primary root growth than *cnx1-1 cnx2-2*, and this phenotype was maintained in the *cnx1-1 cnx2-2 pdr2* triple mutant (Figure 6B). The epistatic action of *lpr1* and *pdr2* over *cnx1-1 cnx2-2* was also observed at the level of Fe accumulation for roots grown under HPi and LPi (Figure 5).

We also examined the effect of overexpressing *PDR2* driven by the CaMV35S promoter. WT and *pdr2* plants overexpressing *PDR2* had significantly longer primary roots compared to those of untransformed WT plants on both HPi and LPi media. By contrast, while *cnx1-1 cnx2-2* double mutant plants overexpressing *PDR2* also had longer primary roots compared to those of WT plants grown under HPi conditions, the same plants showed shorter primary roots than those of WT plants and comparable root lengths to those of the *cnx1-1 cnx2-2* double mutant when grown under LPi conditions (Figure 6C). Overall, these data indicate that the primary root phenotypes of *pdr2* and *lpr1 lpr2* are epistatic to *cnx1-1 cnx2-2* under LPi and that overexpressing *PDR2* failed to rescue the short root phenotype of *cnx1-1 cnx2-2* under LPi.

Quantification of the Pi content in roots of the various mutants used in the epistasis analysis showed no significant differences for plants grown under HPi condition. On LPi, there was a

trend towards lower Pi content in the *lpr1 lpr2* and *cnx1-1 cnx2-2 lpr1 lpr2* mutants compared to WT, although these differences were not statistically significant (Figure 6D).

Pi deficiency induces *CNX* gene expression and ER stress

We examined the expression of *CNX1* and *CNX2* in the shoots and roots of plants grown on LPi and HPi media via reverse transcription quantitative PCR (RT-qPCR). The expression of both *CNX1* and *CNX2* significantly increased under Pi-deficient conditions (Figure 7A). However, the increase in expression for these genes was moderate compared to that of other Pi deficiency–responsive genes, such as *MONOGALACTOSYL DIACYLGLYCEROL SYNTHASE 3* (*MGD3)* and *PHOSPHATE TRANSPORTER 1; 4* (*PHT1;4*) (Figure 7B).

We investigated the transcriptional response of the *cnx1-1 cnx2-2* double mutant to Pi deficiency conditions by examining *MGD3* and *PHT1;4* expression. The expression of both genes in shoots and roots did not significantly differ between *cnx1-1 cnx2-2* and WT on HPi or LPi medium, except that *PHT1;4* was slightly upregulated in *cnx1-1 cnx2-2* shoots on HPi medium (Figure 7B).

The accumulation of mis-folded proteins in the ER leads to ER stress and the increased expression of the transcription factor gene *bZIP60* (Lu and Christopher, 2008). To determine whether LPi treatment leads to ER stress and whether the *cnx1-1 cnx2-2* double mutant exhibits greater signs of ER stress compared to WT plants, we compared the expression of *bZIP60* in *cnx1-1 cnx2-2* versus WT plants grown on HPi and LPi. When we treated plants with the reducing agent dithiothreitol (DTT) to induce ER stress, *bZIP60* was upregulated, with a greater increase in shoots compared to in roots (Figure 7C) (Lu and Christopher, 2008). Under LPi conditions, *bZIP60* expression significantly increased in shoots but not in roots in both WT and *cnx1-1 cnx2-2*, with no significant difference in *bZIP60* expression between these lines (Figure 7C). Thus, the removal of calnexin did not lead to an increase in ER stress compared to the stress level in WT under either HPi or LPi conditions.

Discussion

In the present study, while the *cnx1-1* and *cnx2-2* single mutants showed no defect in primary root growth under HPi or LPi conditions, the *cnx1-1 cnx2-2* double mutant showed reduced primary root growth under LPi but not HPi conditions; this phenotype was complemented by the expression of either *CNX1* or *CNX2* driven by their native promoters. Thus, *CNX1* and *CNX2* are both required and play functionally redundant roles in the response of primary roots to Pi deficiency.

The *cnx1 cnx2* double mutant showed no reduction in secondary root growth as well as no reduction in the capacity of the root system to acquire Pi under LPi or HPi conditions. These features likely explain why the *cnx1 cnx2* mutant shows no reduction in growth or shoot Pi content when grown in soil or clay substrate irrigated with HPi or LPi solution. Under these experimental conditions, differences in primary root length under LPi condition would have an overall minimal impact on the global root mass and capacity of the root system to acquire Pi from the media or soil solution. Similar results have previously been shown for the *pdr2* mutant, which has a stronger primary root growth reduction phenotype on LPi than *cnx1 cnx2* (Ticconi et al., 2004).

Both CNX1 and CNX2 are localized to the ER in Arabidopsis , and the corresponding genes are broadly expressed in most tissues (except that only *CNX1* is substantially expressed in pollen) and throughout development in both shoots and roots (Liu et al., 2017). Previous analysis of higher-order Arabidopsis mutants of *CNX* and *CRT* revealed that while the *cnx1 cnx2* double mutant had no phenotype under normal growth conditions, the *crt1 crt2* double mutant and the *crt1 crt2 crt3* triple mutant showed reduced rosette growth in soil and reduced hypocotyl elongation in the dark (Christensen et al., 2010; Kim et al., 2013; Vu et al., 2017). These results indicate that the CNX and CRT are involved in the folding of at least partially distinct set of client proteins in the ER. CRT3 is a divergent calreticulin within the CRT family and has been shown to contribute to the stability and turnover of several transmembrane receptor-like kinases, such as the brassinosteroid receptor BRI1 as well as the EFR and SOBIR1 receptors involved in plant immunity to bacterial pathogens (Jin et al., 2009; Li et al., 2009; Sun et al., 2014). The absence of primary root phenotype of the *crt1 crt2* and *crt3-1* mutants on LPi indicate that the calreticulins are unlikely to affect folding of the client protein(s) involved in the primary root growth phenotype of the *cnx1 cnx2* mutant.

Analysis of several mutants in genes implicated in the synthesis of the lipid-linked $Glc_3Man9GlcNAc_2$ glycan (*alg3-1*, *alg9a* and *alg10-1*) and its transfer to Asn residues of ER proteins (*stt3a*), the processing/transfer of the terminal glucose moieties (*psl4* and *ebs1-6*), the ERAD pathway (*mns4 mns5*), or various ER molecular chaperones (*sdf2-1*, *bip* mutants) failed to unambiguously reveal defects in primary root growth specifically under LPi conditions. These mutants affect different steps in pathways with distinct consequences on protein folding, protein quality control or protein degradation (Strasser, 2018). PSL4 and EBS1/UGGT are two proteins that are directly involved in the CNX/CRT cycle. The presence of primary root growth phenotypes on HPi for the *psl4* and *ebs1-6* mutants may be masking more subtle effects of the LPi condition. Indeed, *ebs1* mutants have been shown to have strong growth defects affecting both shoots and roots (Blanco-Herrera et al., 2015). Furthermore, mutation in the catalytic alpha subunit of the glucosidase II complex, encoded by the *PSL5* gene, has a strong shoot and root growth phenotype resulting from defects in cellulose biosynthesis (Burn et al., 2002). The role of the non-catalytic ß subunit of glucosidase II, encoded by *PSL4*, in the trimming of glucose residues is currently poorly defined and it is plausible that the carbohydrate binding domain of PSL4 modulates glucosidase II activity only on a subset of CNX/CRT client proteins. It is interesting to note that even highly related glycoproteins may have very distinct requirement for the participation of proteins involved in ER protein folding and quality control. For example, while the leucine-rich repeat receptor kinase (LRR-RK) EFR1 requires the participation of PSL4, PSL5, CRT3 and EBS1/UGGT for optimal activity, the same set of proteins appear not necessary for the activity of the related LRR-RK flagellin receptor FLS2 (Li et al., 2009; Lu et al., 2009). Even structural variants of BRI1 show distinct interactions with the components of the CRT-CNX cycle. Although the BRI1-5 variant interacts with CNX1/CNX2, the *cnx1 cnx2 bri1-5* triple mutant was indistinguishable from the *bri1-5* single mutant, while *ebs1 bri1-5* double mutants had enhanced growth inhibition (Hong et al., 2008). In contrast, the BRI1-9 variant interacts with CRT3 and introgression of either *crt3* or *ebs1* into *bri1-9* suppresses the growth phenotype associated with *bri1-9* (Jin et al., 2007; Jin et al., 2009). Understanding the contribution of various components of the ER protein folding and quality control on the short-root phenotype of the *cnx1 cnx2* mutant will likely require the identification of the CNX1/CNX2-specific client protein(s) affected in the *cnx1 cnx2* mutant that are responsible for this phenotype.

Several mutants we have tested for primary root growth under LPi conditions, including *alg10-1*, *stt3a2*, *ebs1-6*, and *mns4 mns5*, were previously shown to have altered root growth under salt stress (Koiwa et al., 2003; Farid et al., 2011; Huttner et al., 2014; Blanco-Herrera et al., 2015). Considering that the growth of *cnx1-1 cnx2*-2 roots was comparable to that of WT roots under salt stress and osmotic stress, it is likely that defects in different components of the CNX-CRT cycle affect distinct N-glycosylated proteins to different extents. That is, the proteins affected in the *alg10-1*, *stt3a2*, *ebs1-6*, and *mns4 mns5* mutants are involved in the salt stress response, while those affected in *cnx1-1 cnx2-2* are involved in the Pi deficiency response.

While the mode of action of CNX and CRT in ER protein folding has essentially been defined through the binding of the $GlcMan_9GlcNAc_2$ moiety present on N-glycosylated proteins (Strasser, 2018), recent work has demonstrated that CNX can preferentially interact with misfolded non-glycosylated membrane proteins via its single transmembrane domain (Bloemeke et al., 2022). The fact that CNX2 with mutations in key amino acids involved in interacting with the terminal glucose residue of $GlcMan_9GlcNAc_2$ failed to complement the short primary root phenotype of the *cnx1 cnx2* mutant shows that the glycan binding activity of CNX2 to target N-glycosylated client protein(s) is an essential element in the response of primary root growth to LPi. While CRT and CNX bind to both soluble and membrane-bound glycoproteins (Helenius and Aebi, 2004), the recently proposed dual binding mode involving interaction of transmembrane domains and N-glycan dependent binding may distinguish CNX1/CNX2 client proteins from CRT clients (Bloemeke et al., 2022).

The *cnx1 cnx2* mutant shares several features with the *pdr2*, *als3*, and *star1* mutants in terms of their responses to LPi conditions, including Fe-dependent reduced primary root growth associated with a reduction in root meristem size (Ticconi et al., 2004; Müller et al., 2015; Dong et al., 2017). However, the *pdr2*, *als3*, and *star1* mutants have additional root phenotypes under LPi conditions that are not observed in *cnx1-1 cnx2-2*, such as reduced cell length in the root elongation zone and a distorted cellular organization of the root meristem. Furthermore, the *pdr2* mutant was previously shown to have a strongly reduced number of lateral roots and an induction of *PSI* gene expression, such as *PHT1;4* (Ticconi et al., 2004), features that are not observed in the phenotypically milder *cnx1 cnx2* mutant. The apoplastic Fe accumulation (as visualized by Perls-DAB staining) is stronger in *pdr2*, *als3*, and *star1* roots than in *cnx1-1 cnx2-2* roots when grown in LPi in both the elongation and meristematic zones (Ticconi et al., 2004; Müller et al., 2015; Dong et al., 2017). Initial characterization of mutants such as *pdr2*, *lpr1*,

almt1, and *als3* linked strong apoplastic Fe staining in the root meristematic and elongation zones with inhibited cell division and cell elongation. Fe accumulation in the meristem is associated with ROS production, which affects cell wall structure and meristem cell division via reduced mobility of SHORT-ROOT (SHR) in the stem cell niche (Müller et al., 2015; Balzergue et al., 2017). However, a more detailed analysis of dynamic changes in Fe accumulation and primary root growth over time revealed that the extent of primary root growth inhibition cannot simply be directly linked to the level of apoplastic Fe accumulation in the root meristem and elongation zone (Wang et al., 2019). Numerous interactions have been described in the pathways involving Fe and Pi homeostasis, with complex interplay occurring at levels ranging from transport to signaling pathways, which could also impact primary root growth (Hanikenne et al., 2021; Nussaume and Desnos, 2022).

PDR2 encodes a member of the eukaryotic type V subfamily (P5) of P-type ATPase (Ticconi et al., 2009). PDR2 is abundant in the ER, but its mode of action and transport activity are largely unknown, although recent work has reported a role of the yeast P5A ATPase Spf1 in protein translocation in the ER (McKenna et al., 2020). PDR2 is thought to modulate the activity and/or abundance of the ferroxidase LPR1 in the apoplast, which is responsible for the oxidation of Fe^{+2} to Fe^{+3} (Müller et al., 2015; Naumann et al., 2022). Consequently, the *lpr1* phenotypes (in terms of both Fe deposition and reduced primary root growth under LPi conditions) are epistatic to *pdr2* (Ticconi et al., 2009). The *lpr1* phenotypes are also epistatic to *cnx1-1 cnx2-2*. It is unknown if PDR2 is N-glycosylated and if it enters the CNX-CTR cycle. However, considering the milder phenotypes of *cnx1-1 cnx2-2* compared to that of *pdr2* and the finding that overexpressing *PDR2* did not influence the reduced primary root growth of *cnx1 cnx2* on LPi medium, it is unlikely that the root growth phenotype of *cnx1-1 cnx2-2* is mediated by reduced PDR2 activity.

The lack of calnexin leads to a range of phenotypes in fungi and animals, from lethality in the yeast *Schizosaccharomyces pombe* to developmental and neurological abnormalities in zebrafish, mouse, and Drosophila (Parlati et al., 1995; Kraus et al., 2010; Hung et al., 2013; Xiao et al., 2017). The current study highlights a role for calnexin in the response of primary root growth to Pi deficiency. Phosphate deficiency has been associated with an increase in autophagy in root tips and leaves as well as an increase in *CNX1* and *BiP2* expression (Naumann et al., 2019; Yoshitake et al., 2021). Here, Pi deficiency resulted in the increased expression of *CNX1* and *CNX2* in both roots and shoots as well as *bZIP60* in shoots. Collectively, these data

505 reveal that Pi deficiency is associated with an increase in ER stress. Yet, the absence of a
506 substantial difference in *bZIP60* expression between WT and the *cnx1-1 cnx2-2* double mutant
507 indicates that the absence of calnexin in Arabidopsis does not lead to a systematic increase in
508 ER stress responses, at least under HPi or LPi conditions. This implies that the folding and
509 activity of a restricted number of N-glycosylated proteins are likely affected by the absence of
510 calnexin; one or a few of these proteins likely contribute to the reduced primary root growth
511 under LPi conditions.
512
513
514
515

Materials and Methods

Plant lines and growth conditions

Arabidopsis (*Arabidopsis thaliana*) seeds were surface sterilized and grown for 7 days on plates containing half-strength Murashige and Skoog (MS) medium without phosphate (Caisson Laboratories) supplemented with 75 μM or 1 mM KH_2PO_4 buffer (pH 5.8), 1% (w/v) sucrose, 0.7% (w/v) agarose, and 500 mg/L 2-(N-morpholino) ethanesulfonic acid (final pH 5.8). To induce different levels of phosphate and iron deficiency, ferrozine was added to the medium at a final concentration of 100 μM. Plants were grown vertically on plates at 22°C under a continuous light intensity of 100 μmol m^{-2} s^{-1}.

Plants were also grown in soil or in a clay-based substrate (Seramis) irrigated with phosphate-free half-strength MS supplemented with KH_2PO_4 buffer, pH 5.8. The growth chamber conditions were 22°C and 60% relative humidity with a 16-h-light/8-h-dark photoperiod with 100 μE/m^2 per s of white light.

All Arabidopsis lines used in this study are in the Col-0 background. A single *cnx1* (SALK_083600C) allele and two *cnx2* (SAIL_865_F08 and SAIL_580_H02) mutant alleles were identified from T-DNA insertional lines obtained from the European Arabidopsis Stock Center (NASC) (http://arabidopsis.info). Supplemental Table S1 lists the sources of all other lines used in this study. Plants overexpressing *PDR2* under the control of the CaMV35S promoter (Ticconi et al., 2009) as well as plants expressing the reporter construct cycB1::GUS (Colon-Carmona et al., 1999) were described previously.

Phosphate quantification

Quantification of Pi was performed as previously described (Ames, 1966). Shoot or root material was placed in pure water, and at least three freeze-thaw cycles were applied to release the inorganic Pi, which was quantified via a molybdate assay using a standard curve. For Pi quantification of seedlings, four biological replicates per condition were utilized, where tissues from 20 seedlings were pooled together. The statistical differences were assessed by two-way ANOVAs followed by a Tukey's tests. For Pi quantification on plants grown in soil, tissue from individual plants was collected as biological replicates (8-10 replicates per condition were used). The statistical differences were analyzed by Student's *t*-tests.

549

550 **DNA constructs and gene expression analysis**

551 PCR-generated fragments of the *CNX1* and *CNX2* genomic regions lacking stop codons and
552 including the 1-kbp promoter regions were obtained using Phusion HF DNA polymerase (New
553 England Biolabs), inserted into pENTR-2B, and recombined in pMDC107 to generate the GFP-
554 tagged construct using Gateway technology. Generation of the Y122A and K124A point
555 mutants in the construct *pCNX2::CNX-GFP* was performed by gene synthesis (GenScript
556 Biotech, Netherlands). The various binary vectors were introduced into Arabidopsis plants via
557 *Agrobacterium tumefaciens*–mediated transformation using the floral dip method (Clough and
558 Bent, 1998).
559
560 Total RNA was extracted from roots or shoots using an RNA Purification kit as described by
561 the manufacturer (Promega), followed by DNase I treatment. cDNA was synthesized from 1
562 µg of RNA using M-MLV Reverse Transcriptase (Promega) and oligo $d(T)_{15}$ following the
563 manufacturer's instructions. RT-qPCR analysis was performed using SYBR Select Master Mix
564 (Applied Biosystems) with primer pairs specific to genes of interest; *ACT2* was used for data
565 normalization. The primer sequences are listed in Supplemental Table S2. Three biological
566 replicates per condition were used, each one consisting of a pool of approximately 60 seedlings.
567 Significant differences in gene expression levels were analyzed using Student's *t*-tests.
568

569 **Root measurements, microscopy, and staining procedures**

570 Root length was measured using seedlings grown on vertically oriented plates. The plates were
571 scanned on a flatbed scanner to produce image files suitable for quantitative analysis using
572 ImageJ software (v1.44p).
573
574 Confocal microscopy was performed using a Zeiss LSM 880 confocal laser scanning
575 microscope. Plant roots were treated with Clearsee solution and stained with calcofluor white
576 (Ursache et al., 2018) to visualize cell walls. A line expressing the cycB1::GUS reporter was
577 used to introgress the construct into the *cnx1-1 cnx2-2* double mutant background. Roots were
578 stained for GUS activity as previously described (Lagarde et al., 1996). The tissues were
579 vacuum infiltrated to enhance tissue penetration. Stained tissues were cleared in chloral hydrate
580 solution (2.7 g/mL in 30% (v/v) glycerol) and analyzed using a Leica DM5000B bright-field
581 microscope.

582

583 Iron accumulation in seedlings was assayed by Perls-DAB staining as previously described
584 (Müller et al., 2015). Briefly, seedlings were incubated in 4 mL of 2% (v/v) HCl and 2% (w/v)
585 potassium ferrocyanide for 30 min. The samples were washed with water and incubated for 45
586 min in 4 mL of 10 mM NaN_3 and 0.3% H_2O_2 (v/v) in methanol. The samples were then washed
587 with 100 mM Na-phosphate buffer (pH 7.4) and incubated for 30 min in the same buffer
588 containing 0.025% (w/v) DAB and 0.005% (v/v) H_2O_2. Finally, the samples were washed twice
589 with water, cleared with chloral hydrate (1 g/mL, 15% glycerol (v/v), and analyzed using an
590 optical microscope.
591

592 **Immunoblot analysis**

593 Proteins were extracted from homogenized plant material at 4°C in extraction buffer containing
594 10 mM phosphate buffer (pH 7.4), 300 mM sucrose, 150 mM NaCl, 5 mM EDTA, 5 mM
595 EGTA, 1 mM DTT, 20 mM NaF, and 1× protease inhibitor (Roche EDTA Free Complete Mini
596 Tablet) and sonicated for 10 min in an ice-cold water bath. Fifty micrograms of proteins were
597 separated by SDS-PAGE and transferred to an Amersham Hybond-P PVDF membrane (GE
598 Healthcare). The membrane was probed with rabbit polyclonal antibodies against maize
599 calreticulin, which cross-reacts with both Arabidopsis calnexin and calreticulin (Persson et al.,
600 2003), and goat anti-rabbit IgG-HRP (Santa Cruz Biotechnology) using Western Bright Sirius
601 HRP substrate (Advansta). Signal intensity was measured using a GE Healthcare ImageQuant
602 RT ECL Imager.

603

604 **Accession Numbers**
605 Sequence data from this article can be found in The Arabidopsis Information Resource
606 (www.arabidopsis.org) using the gene codes as defined in Supplemental Table S1.

607 **Supplemental Data**

608 Supplemental Figure S1. Phenotype of the *cnx1 cnx2* double mutant under high and low Pi
609 conditions.

610 Supplemental Figure S2. Localization of *CNX1::CNX1-GFP* and *CNX2::CNX2-GFP* in the ER.

Supplemental Figure S3. Amino acid alignment between the CNX2 and CRT3 of Arabidopsis and the mouse CRT3.

Supplemental Table S1. List of mutants used in this work.

Supplemental Table S2. Primer list.

Funding information

This work was supported by Swiss National Science Foundation (Schweizerische Nationalfonds) grants 31003A-182462 and 31003A-159998 to Y.P.

Acknowledgments

The authors are grateful to Shuh-ichi Nishikawa (Niigata University, Japan), Cyril Zipfel (University of Zurich, Switzerland) and Thierry Desnos (CEA-Cadarache, France) for seeds of the *bip*, *sdf2* and *lpr1 lpr2* mutants, respectively.

Competing interests

None

631 **Figure legends**

632

633 **Figure 1. Phenotype of the *cnx1 cnx2* double mutant under high and low Pi conditions.**
634 **(A)** Schematic diagram of the T-DNA insertions in the *CNX1* (At5g61790) and *CNX2*
635 (At5g07340) genes in the *cnx* mutants. Exons are shown as black boxes. **(B)** Immunoblot
636 analysis of CNX and CRT in whole protein extracts from seedlings. The position of the 70 KDa
637 molecular weight marker is shown on the right. **(C)** Primary root length of WT compared to
638 that of the *cnx1-1* and *cnx2-2* single and double mutants. Plants were grown for 7 days on plates
639 containing 1 mM Pi (HPi) or 75 µM Pi (LPi) before measuring primary root length. **(D)**
640 Complementation of the primary root phenotype of *cnx1-1 cnx2-2* plants transformed with the
641 CNX1:GFP or CNX2:GFP construct. **(E)** Representative photos of plants analyzed in C and D
642 grown on HPi and LPi plates. Bars represent 1 cm. **(F-G)** Length (F) and density (G) of lateral
643 roots (LRs) of WT compared to those of the *cnx1-1 cnx2-2* double mutant for plants on agar-
644 solidified medium with HPi and LPi for 10 days. In C and D, statistical analysis was performed
645 by two-way ANOVA followed by a Tukey's test, and significant differences compared to WT
646 in each growth condition are shown. In F and G, differences between WT and *cn1-1 cnx2-2*
647 were assessed by an unpaired t-test. **, $P < 0.01$; ***, $P < 0.001$; ****, $P < 0.0001$; error bars
648 = SD; $n \geq 9$.

649

650

651 **Figure 2. Primary root growth of mutants in genes involved in ER protein synthesis and**
652 **quality control. (A-B)** Plants were grown for 7 days on plates containing HPi or LPi before
653 measuring primary root length. **(C-D)** Primary root length of WT and *cnx1-1 cnx2-2* plants after
654 7 days of growth on HPi plates (C) without or with 200 mM mannose or (D) without or with
655 100 mM NaCl. **(E-F)** Primary root length of WT and *cnx1-1 cnx2-2* after 7 days of growth on
656 plates containing HPi or LPi half-strength MS medium or the same medium with ferrozine to
657 chelate Fe (HPi -Fe and LPi -Fe). Statistical analysis was performed by two-way ANOVA
658 followed by a Tukey's test, and significant differences compared to WT in each growth
659 condition are shown, *$P < 0.05$, **$P < 0.01$, ***$P < 0.001$, ****$P < 0.0001$, error bars = SD, n
660 ≥ 5. Bar represents 1 cm in F.

661

662 **Figure 3. Mutations in the glycan binding domain of CNX2 abolish its ability to**
663 **complement the *cnx1-1 cnx2-2* mutant phenotype. (A)** Alignment of segments of CNX2 and
664 CRT3 from Arabidopsis (AtCNX2, AtCRT3) and CRT from mouse (MmCRT). The key amino

acids Y122 and K124 from the AtCNX2 targeted by mutagenesis are highlighted by red arrows. The table on the right shows the equivalence in the position of the key tyrosine and lysine residues in AtCNX2, AtCRT3 and MmCRT. (B) Primary root length of *cnx1-1 cnx2-2* parental plants and transgenic *cnx1-1 cnx2-2* transformed with the wild type (WT), Y122A or K124A mutant versions of the construct pCNX2::CNX2-GFP. Plants were grown for 7 days on plates containing 1 mM Pi (HPi) or 75 µM Pi (LPi) before measuring primary root length. Error bars = SD. Statistical analysis was performed by one-way ANOVA followed by a Tukey's test; different letters indicate a significant difference with a *P*-value<0.05. Bars in the left photo represents 1 cm. (C) Confocal images of GFP expression of WT, Y122A or K124A mutant versions of the construct pCNX2::CNX2-GFP in roots tips of transgenic *cnx1-1 cnx2-2* plants. Bars = 25 µm, applies to all images.

Figure 4. The *cnx1-1 cnx2-2* double mutant is affected in meristem activity. (A-C) Plants were grown for 7 days on plates containing 1 mM Pi (HPi) or 75 µM Pi (LPi) before measuring the length of the cell division zone in the meristem (A, B), defined in A by the yellow and red arrows, and cell length in the differentiation zone (C). Statistical analysis (B, C) was performed by two-way ANOVA followed by a Tukey's test; significant differences compared to WT under each growth condition are shown: ****, $P < 0.0001$; error bars = SD; $n \geq 5$ in (B) and 20 in (C). **(D)** WT and *cnx1-1 cnx2-2* plants transformed with the cylinB1:GUS reporter gene construct were grown for 7 days on plates containing HPi or LPi medium and stained for β-glucuronidase activity. Bars represent 50 um in A and 100 µm in D.

Figure 5. Fe accumulation and distribution in the roots of mutants grown under high and low Pi conditions. Plants were grown for 7 days on plates containing 1 mM Pi (HPi) or 75 µM Pi (LPi) and subjected to Perls-DAB staining for Fe visualization. Bar represents 1 mm.

Figure 6. Epistatic interactions among *cnx1-1 cnx2-2*, *lpr1-1 lpr2-1*, and *pdr2*. Plants were grown for 7 days on 1 mM Pi (HPi) or 75 µM Pi (LPi) plates before recording primary root length. **(A)** Epistatic interaction between *cnx1-1 cnx2-2* and *lpr1-1 lpr2-1*. **(B)** Epistatic interaction between *cnx1-1 cnx2-2* and *pdr2*. **(C)** A T-DNA cassette for *PDR2* overexpression under the control of the CaMV35S promoter (OEPDR2) was introgressed into Col-0, *cnx1-1 cnx2-2*, and *pdr2*. **(D)** Pi content in roots for plants grown for 7 days on HPi or LPi. Statistical analysis was performed by two-way ANOVA followed by a Tukey's test, and significant

differences within each growth condition are shown. Different lowercase letters (a, b, c, or d) indicate a significant difference with a *P*-value < 0.05, n ≥ 6, error bars = SD.

Figure 7. Impact of the *cnx1-1 cnx2-2* mutations on the expression of Pi deficiency and unfolded protein response marker genes. (A) *CNX1* and *CNX*2 expression in the shoots and roots of plants grown for 7 days in 1 mM Pi (HPi) or 75 µM Pi (LPi) medium. (B) Expression of the Pi deficiency markers *MGD3* and *PHT1;4* in the shoots and roots of WT and *cnx1-1 cnx2-2* grown for 7 days on HPi or LPi medium. (C) Induction of ER unfolded protein response marker gene *bZIP60* in the shoots and roots of WT at 24 h after the addition of 2 mM DTT and in the *cnx1-1 cnx2-2* double mutant compared to WT grown under HPi or LPi conditions. Statistical analysis was performed by Student's *t*-test comparing different treatments (HPi and LPi for A and C, Control and DTT for C) and WT vs. *cnx1-1 cnx2-2* (B, C), with significant differences indicated by asterisks:*, $P < 0.05$; **, $P < 0.01$; ***, $P < 0.001$. Error bars = SD, n = 3.

References

Ames BN (1966) Assay of inorganic phosphate, total phosphate and phosphatases. Methods Enzymol **8:** 115-118

Balzergue C, Dartevelle T, Godon C, Laugier E, Meisrimler C, Teulon JM, Creff A, Bissler M, Brouchoud C, Hagege A, et al (2017) Low phosphate activates STOP1-ALMT1 to rapidly inhibit root cell elongation. Nature Commun **8:** 15300

Blanco-Herrera F, Moreno AA, Tapia R, Reyes F, Araya M, D'Alessio C, Parodi A, Orellana A (2015) The UDP-glucose: glycoprotein glucosyltransferase (UGGT), a key enzyme in ER quality control, plays a significant role in plant growth as well as biotic and abiotic stress in *Arabidopsis thaliana*. BMC Plant Biol **15:** 127

Bloemeke N, Meighen-Berger K, Hitzenberger M, Bach NC, Parr M, Coelho JP, Frishman D, Zacharias M, Sieber SA, Feige MJ (2022) Intramembrane client recognition potentiates the chaperone functions of calnexin. EMBO J **e110959**

Brandizzi F (2021) Maintaining the structural and functional homeostasis of the plant endoplasmic reticulum. Dev Cell **56:** 919-932

Burn JE, Hurley UA, Birch RJ, Arioli T, Cork A, Williamson RE (2002) The cellulose-deficient Arabidopsis mutant rsw3 is defective in a gene encoding a putative glucosidase II, an enzyme processing N-glycans during ER quality control. Plant J **32:** 949-960

Chen Q, Yu FF, Xie Q (2020) Insights into endoplasmic reticulum-associated degradation in plants. New Phytol **226:** 345-350

Christensen A, Svensson K, Thelin L, Zhang WJ, Tintor N, Prins D, Funke N, Michalak M, Schulze-Lefert P, Saijo Y, et al (2010) Higher plant calreticulins have acquired specialized functions in Arabidopsis. Plos One **5:** e11342

Clough SJ, Bent AF (1998) Floral dip: a simplified method for *Agrobacterium*-mediated transformation of *Arabidopsis thaliana*. Plant J **6:** 735-743

Colon-Carmona A, You R, Haimovitch-Gal T, Doerner P (1999) Spatio-temporal analysis of mitotic activity with a labile cyclin-GUS fusion protein. Plant J **20:** 503-508

Crombez H, Motte H, Beeckman T (2019) Tackling plant phosphate starvation by the roots. Dev Cell **48:** 599-615

Deng Y, Humbert S, Liu JX, Srivastava R, Rothstein SJ, Howell SH (2011) Heat induces the splicing by IRE1 of a mRNA encoding a transcription factor involved in the unfolded protein response in Arabidopsis. Proc Natl Acad Sci USA **108:** 7247-7252

748 **Dissanayaka DMSB, Ghahremani M, Siebers M, Wasaki J, Plaxton WC** (2021) Recent
749 insights into the metabolic adaptations of phosphorus-deprived plants. J Exp Bot **72:**
750 199-223
751 **Dong JS, Pineros MA, Li XX, Yang HB, Liu Y, Murphy AS, Kochian LV, Liu D** (2017)
752 An Arabidopsis ABC transporter mediates phosphate deficiency-induced remodeling of
753 root architecture by modulating iron homeostasis in roots. Mol Plant **10:** 244-259
754 **Farid A, Pabst M, Schoberer J, Altmann F, Glossl J, Strasser R** (2011) *Arabidopsis thaliana*
755 alpha1,2-glucosyltransferase (ALG10) is required for efficient N-glycosylation and leaf
756 growth. Plant J **68:** 314-325
757 **Gao HB, Brandizzi F, Benning C, Larkin RM** (2008) A membrane-tethered transcription
758 factor defines a branch of the heat stress response in *Arabidopsis thaliana*. Proc Natl
759 Acad Sci USA **105:** 16398-16403
760 **Gutierrez-Alanis D, Yong-Villalobos L, Jimenez-Sandoval P, Alatorre-Cobos F, Oropeza-**
761 **Aburto A, Mora-Macias J, Sanchez-Rodriguez F, Cruz-Ramirez A, Herrera-**
762 **Estrella L** (2017) Phosphate starvation-dependent iron mobilization induces CLE14
763 expression to trigger root meristem differentiation through CLV2/PEPR2 signaling.
764 Dev Cell **41:** 555-570
765 **Hanikenne M, Esteves SM, Fanara S, Rouached H** (2021) Coordinated homeostasis of
766 essential mineral nutrients: a focus on iron. J Exp Bot **72:** 2136-2153
767 **Helenius A, Aebi M** (2004) Roles of N-linked glycans in the endoplasmic reticulum. Annu
768 Rev Biochem **73:** 1019-1049
769 **Hong Z, Jin H, Tzfira T, Li JM** (2008) Multiple mechanism-mediated retention of a defective
770 brassinosteroid receptor in the endoplasmic reticulum of Arabidopsis. Plant Cell **20:**
771 3418-3429
772 **Hong Z, Kajiura H, Su W, Jin H, Kimura A, Fujiyama K, Li JM** (2012) Evolutionarily
773 conserved glycan signal to degrade aberrant brassinosteroid receptors in Arabidopsis.
774 Proc Natl Acad Sci USA **109:** 11437-11442
775 **Hung IC, Cherng BW, Hsu WM, Lee SJ** (2013) Calnexin is required for zebrafish posterior
776 lateral line development. Int J Dev Biol **57:** 427-438
777 **Huttner S, Veit C, Vavra U, Schoberer J, Liebminger E, Maresch D, Grass J, Altmann F,**
778 **Mach L, Strasser R** (2014) Arabidopsis class I alpha-mannosidases MNS4 and MNS5
779 are involved in endoplasmic reticulum-associated degradation of misfolded
780 glycoproteins. Plant Cell **26:** 1712-1728

Jin H, Hong Z, Su W, Li JM (2009) A plant-specific calreticulin is a key retention factor for a defective brassinosteroid receptor in the endoplasmic reticulum. Proc Natl Acad Sci USA **106:** 13612-13617

Jin H, Yan Z, Nam KH, Li JM (2007) Allele-specific suppression of a defective brassinosteroid receptor reveals a physiological role of UGGT in ER quality control. Mol Cell **26:** 821-830

Joshi R, Paul M, Kumar A, Pandey D (2019) Role of calreticulin in biotic and abiotic stress signalling and tolerance mechanisms in plants. Gene **714:** 144004

Kajiura H, Seki T, Fujiyama K (2010) *Arabidopsis thaliana alg3* mutant synthesizes immature oligosaccharides in the ER and accumulates unique N-glycans. Glycobiol **20:** 736-751

Kapoor M, Ellgaard L, Gopalakrishnapai J, Schirra C, Gemma E, Oscarson S, Helenius A, Surolia A (2004) Mutational analysis provides molecular insight into the carbohydrate-binding region of calreticulin: Pivotal roles of tyrosine-109 and aspartate-135 in carbohydrate recognition. Biochemistry **43:** 97-106

Kim JH, Nguyen NH, Nguyen NT, Hong SW, Lee H (2013) Loss of all three calreticulins, CRT1, CRT2 and CRT3, causes enhanced sensitivity to water stress in Arabidopsis. Plant Cell Rep **32:** 1843-1853

Koiwa H, Li F, McCully MG, Mendoza I, Koizumi N, Manabe Y, Nakagawa Y, Zhu JH, Rus A, Pardo JM, et al (2003) The STT3a subunit isoform of the Arabidopsis oligosaccharyltransferase controls adaptive responses to salt/osmotic stress. Plant Cell **15:** 2273-2284

Kozlov G, Gehring K (2020) Calnexin cycle - structural features of the ER chaperone system. FEBS J **287:** 4322-4340

Kozlov G, Pocanschi CL, Rosenauer A, Bastos-Aristizabal S, Gorelik A, Williams DB, Gehring K (2010) Structural basis of carbohydrate recognition by calreticulin. J Biol Chem **285:** 38612-38620

Kraus A, Groenendyk J, Bedard K, Baldwin TA, Krause KH, Dubois-Dauphin M, Dyck J, Rosenbaum EE, Korngut L, Colley NJ, et al (2010) Calnexin deficiency leads to dysmyelination. J Biol Chem **285:** 18928-18938

Lagarde D, Basset M, Lepetit M, Conejero G, Gaymard F, Astruc S, Grignon C (1996) Tissue-specific expression of Arabidopsis *AKT1* gene is consistent with a role in K+ nutrition. Plant J **9:** 195-203

Li J, Zhao-Hui C, Batoux M, Nekrasov V, Roux M, Chinchilla D, Zipfel C, Jones JDG (2009) Specific ER quality control components required for biogenesis of the plant innate immune receptor EFR. Proc Natl Acad Sci USA **106:** 15973-15978

Liu DYT, Smith PMC, Barton DA, Day DA, Overall RL (2017) Characterisation of Arabidopsis calnexin 1 and calnexin 2 in the endoplasmic reticulum and at plasmodesmata. Protoplasma **254:** 125-136

Liu J-X, Howell SH (2010) Endoplasmic reticulum protein quality control and its relationship to environmental stress responses in plants. Plant Cell **22:** 2930-2942

Liu J-X, Howell SH (2016) Managing the protein folding demands in the endoplasmic reticulum of plants. New Phytol **211:** 418-428

Liu YD, Li JM (2013) An in vivo investigation of amino acid residues critical for the lectin function of Arabidopsis Calreticulin 3. Mol Plant **6:** 985-987

Lu DP, Christopher DA (2008) Endoplasmic reticulum stress activates the expression of a sub-group of protein disulfide isomerase genes and AtbZIP60 modulates the response in *Arabidopsis thaliana*. Mol Genet Genomics **280:** 199-210

Lu X, Tintor N, Mentzel T, Kombrink E, Boller T, Robatzek S, Schulze-Lefert P, Saijo Y (2009) Uncoupling of sustained MAMP receptor signaling from early outputs in an Arabidopsis endoplasmic reticulum glucosidase II allele. Proc Natl Acad Sci USA **106:** 22522-22527

Manghwar H, Li J (2022) Endoplasmic reticulum stress and unfolded protein response signaling in plants. Int J Mol Sci **23:** 477-499

Maruyama D, Sugiyama T, Endo T, Nishikawa S (2014) Multiple BiP genes of *Arabidopsis thaliana* are required for male gametogenesis and pollen competitiveness. Plant Cell Physiol **55:** 801-810

McKenna MJ, Sim SI, Ordureau A, Wei LJ, Harper JW, Shao SC, Park E (2020) The endoplasmic reticulum P5A-ATPase is a transmembrane helix dislocase. Science **369:** eabc5809

Mora-Macias J, Ojeda-Rivera JO, Gutierrez-Alanis D, Yong-Villalobos L, Oropeza-Aburto A, Raya-Gonzalez J, Jimenez-Dominguez G, Chavez-Calvillo G, Rellan-Alvarez R, Herrera-Estrella L (2017) Malate-dependent Fe accumulation is a critical checkpoint in the root developmental response to low phosphate. Proc Natl Acad Sci USA **114:** E3563-E3572

Müller J, Toev T, Heisters M, Teller J, Moore KL, Hause G, Dinesh DC, Burstenbinder K, Abel S (2015) Iron-dependent callose deposition adjusts root meristem maintenance to phosphate availability. Dev Cell **33:** 216-230

Naumann C, Heisters M, Brandt W, Janitza P, Alfs C, Tang N, Nienguesso AT, Ziegler J, Imre R, Mechtler K, et al (2022) Bacterial-type ferroxidase tunes iron-dependent phosphate sensing during Arabidopsis root development. Curr Biol **32:** 2189–2205

Naumann C, Mueller J, Sakhonwasee S, Wieghaus A, Hause G, Heisters M, Buerstenbinder K, Abel S (2019) The local phosphate deficiency response activates endoplasmic reticulum stress-dependent autophagy. Plant Physiol **179:** 460-476

Nekrasov V, Li J, Batoux M, Roux M, Chu ZH, Lacombe S, Rougon A, Bittel P, Kiss-Papp M, Chinchilla D, et al (2009) Control of the pattern-recognition receptor EFR by an ER protein complex in plant immunity. EMBO J **28:** 3428-3438

Nussaume L, Desnos T (2022) "Je t'aime moi non plus": A love-hate relationship between iron and phosphate. Mol Plant **15:** 1-2

Park CJ, Park JM (2019) Endoplasmic reticulum plays a critical role in integrating signals generated by both biotic and abiotic stress in plants. Front Plant Sci **10:** 399

Parlati F, Dignard D, Bergeron JJM, Thomas DY (1995) The calnexin homolog cnx1(+) in *Schizosaccharomyces pombe*, is an essential gene which can be complemented by its soluble ER domain. EMBO J **14:** 3064-3072

Persson S, Rosenquist M, Svensson K, Galvao R, Boss WF, Sommarin M (2003) Phylogenetic analyses and expression studies reveal two distinct groups of calreticulin isoforms in higher plants. Plant Physiol **133:** 1385-1396

Poirier Y, Jaskolowski A, Clua J (2022) Phosphate acquisition and metabolism in plants. Curr Biol **32:** R623-R629

Reyes-Impellizzeri S, Moreno AA (2021) The endoplasmic reticulum role in the plant response to abiotic stress. Front Plant Sci **12:** 755447-755447

Stephani M, Picchianti L, Gajic A, Beveridge R, Skarwan E, Hernandez VSD, Mohseni A, Clavel M, Zeng YL, Naumann C, et al (2020) A cross-kingdom conserved ER-phagy receptor maintains endoplasmic reticulum homeostasis during stress. Elife **9:** e58396

Strasser R (2018) Protein quality control in the endoplasmic reticulum of plants. Annu Rev Plant Biol **69:** 147-172

878 **Sun TJ, Zhang Q, Gao MH, Zhang YL** (2014) Regulation of SOBIR1 accumulation and
879 activation of defense responses in bir1-1 by specific components of ER quality control.
880 Plant J **77:** 748-756
881 **Svistoonoff S, Creff A, Reymond M, Sigoillot-Claude C, Ricaud L, Blanchet A, Nussaume**
882 **L, Desnos T** (2007) Root tip contact with low-phosphate media reprograms plant root
883 architecture. Nat Genet **39:** 792-796
884 **Thomson SP, Williams DB** (2005) Delineation of the lectin site of the molecular chaperone
885 calreticulin. Cell Stress Chaperon **10:** 242-251
886 **Ticconi C, Lucero R, Sakhonwasee S, Adamson A, Creff A, Nussaume L, Desnos T, Abel**
887 **S** (2009) ER-resident proteins PDR2 and LPR1 mediate the developmental response of
888 root meristems to phosphate availability. Proc Natl Acad Sci USA **106:** 14174-14179
889 **Ticconi CA, Abel S** (2004) Short on phosphate: plant surveillance and countermeasures.
890 Trends Plant Sci **9**
891 **Ticconi CA, Delatorre CA, Lahner B, Salt DE, Abel S** (2004) Arabidopsis pdr2 reveals a
892 phosphate-sensitive checkpoint in root development. Plant J **37:** 801-814
893 **Ursache R, Andersen TG, Marhavy P, Geldner N** (2018) A protocol for combining
894 fluorescent proteins with histological stains for diverse cell wall components. Plant J
895 **93:** 399-412
896 **Vu KV, Nguyen VT, Jeong CY, Lee YH, Lee H, Hong SW** (2017) Systematic deletion of the
897 ER lectin chaperone genes reveals their roles in vegetative growth and male
898 gametophyte development in Arabidopsis. Plant J **89:** 972-983
899 **Wang XY, Wang Z, Zheng Z, Dong JS, Song L, Sui LQ, Nussaume L, Desnos T, Liu D**
900 (2019) Genetic dissection of Fe-dependent signaling in root developmental responses
901 to phosphate deficiency. Plant Physiol **179:** 300-316
902 **Xiao X, Chen CY, Yu TM, Ou JY, Rui ML, Zhai YF, He YJ, Xue L, Ho MS** (2017)
903 Molecular chaperone calnexin regulates the function of Drosophila sodium channel
904 paralytic. Front Mol Neurosci **10**
905 **Yoshitake Y, Nakamura S, Shinozaki D, Izumi M, Yoshimoto K, Ohta H, Shimojima M**
906 (2021) RCB-mediated chlorophagy caused by oversupply of nitrogen suppresses
907 phosphate-starvation stress in plants. Plant Physiol **185:** 318-330
908
909

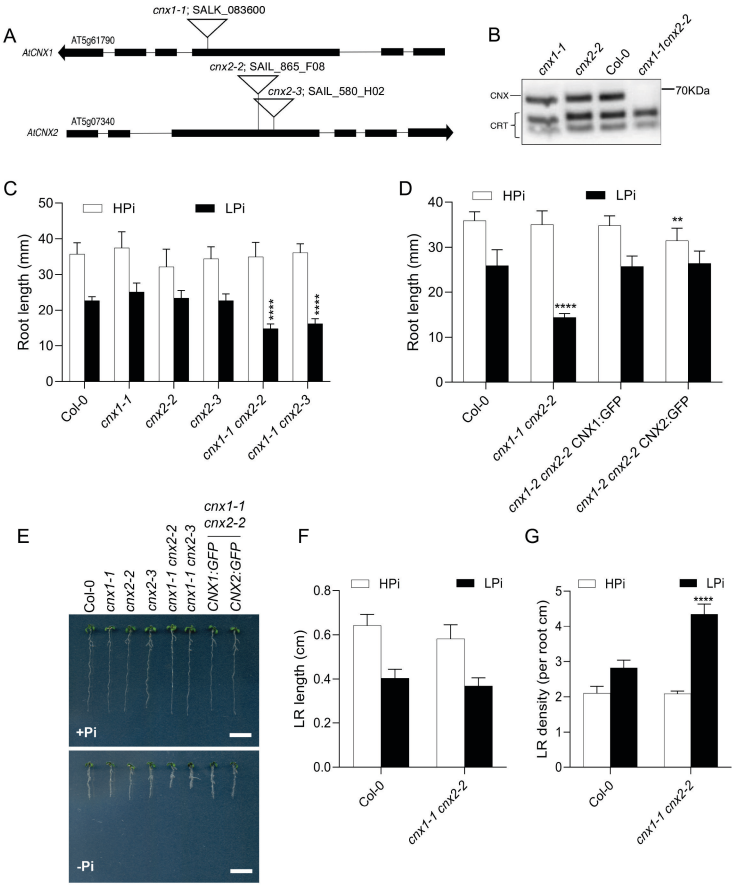

Figure 1. Phenotype of the *cnx1 cnx2* double mutant under high and low Pi conditions. (A) Schematic diagram of the T-DNA insertions in the CNX1 (At5g61790) and CNX2 (At5g07340) genes in the cnx mutants. Exons are shown as black boxes. (B) Immunoblot analysis of CNX and CRT in whole protein extracts from seedlings. The position of the 70 KDa molecular weight marker is shown on the right. (C) Primary root length of Col-0 compared to cnx1-1 and cnx2-2 single and double mutants. Plants were grown for 7 days on plates containing 1 mM Pi (HPi) or 75 µM Pi (LPi) before measuring primary root length.
(D) Complementation of the primary root phenotype of cnx1-1 cnx2-2 plants transformed with the CNX1:GFP or CNX2:GFP construct.
(E) Representative photo of plants analyzed in C and D grown on HPi and LPi plates. Bars represent 1 cm. (F-G) Length (F) and density (G) of lateral roots of Col-0 compared to cnx1-1 cnx2-2 double mutant for plants on agar-solidified medium with HPi and LPi for 10 days.
In C and D, statistical analysis was performed by two-way ANOVA followed by a Tukey's test, and significant differences compared to Col-0 in each growth condition are shown. In F and G, differences between Col-0 and cn1-1 cnx2-2 were assessed by an unpaired t-test. **, $P < 0.01$; ***, $P < 0.001$; ****, $P < 0.0001$; error bars = SD; $n \geq 9$.

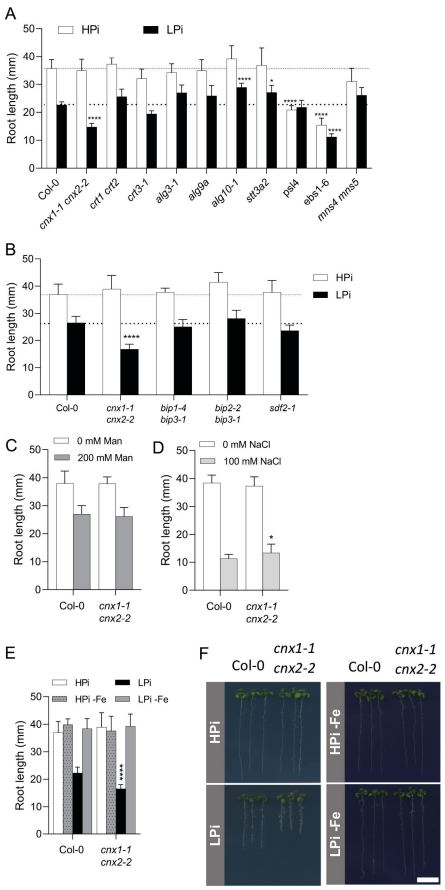

Figure 2. Primary root growth of mutants in genes involved in ER protein synthesis and quality control. (A-B) Plants were grown for 7 days on plates containing HPi or LPi before measuring primary root length. (C-D) Primary root length of Col-0 and cnx1-1 cnx2-2 plants after 7 days of growth on HPi plates (C) without or with 200 mM mannose or (D) without or with 100 mM NaCl. (E-F) Primary root length of Col-0 and cnx1-1 cnx2-2 after 7 days of growth on plates containing HPi or LPi half-strength MS medium or the same medium with ferrozine to chelate Fe (HPi -Fe and LPi -Fe). Statistical analysis was performed by two-way ANOVA followed by a Tukey's test, and significant differences compared to Col-0 in each growth condition are shown, *P < 0.05, **P < 0.01, ***P < 0.001, ****P < 0.0001, error bars = SD, n ≥ 5. Bar represents 1 cm in F.

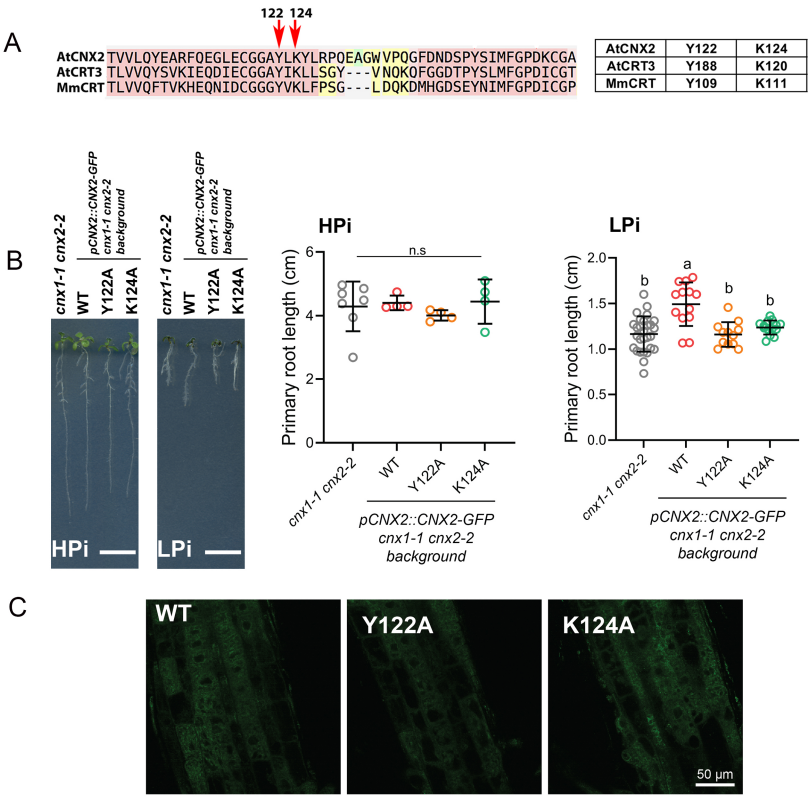

Figure 3. Mutations in the glycan binding domain of CNX2 abolish its ability to complement the cnx1-1 cnx2-2 mutant phenotype. (A) Alignment of segments of CNX2 and CRT3 from A. thaliana (AtCNX2, AtCRT3) and CRT from mouse (MmCRT). The key amino acids Y122 and K124 from the AtCNX2 targeted by mutagenesis are highlighted by red arrows. The table on the right shows the equivalence in the position of the key tyrosine and lysine residues in AtCNX2, AtCRT3 and MmCRT. (B) Primary root length of cnx1-1 cnx2-2 parental plants and transgenic cnx1-1 cnx2-2 transformed with the wild type (WT), Y122A or K124A mutant versions of the construct pCNX2::CNX2-GFP. Plants were grown for 7 days on plates containing 1 mM Pi (HPi) or 75 µM Pi (LPi) before measuring primary root length. Error bars = SD. Statistical analysis was performed by one-way ANOVA followed by a Tukey's test; different letters indicate a significant difference with a p-value<0.05. Bars in the left photo represents 1 cm. (C) Confocal images of GFP expression of WT, Y122A or K124A mutant versions of the construct pCNX2::CNX2-GFP in roots tips of transgenic cnx1-1 cnx2-2 plants. Bars = 10 µm.

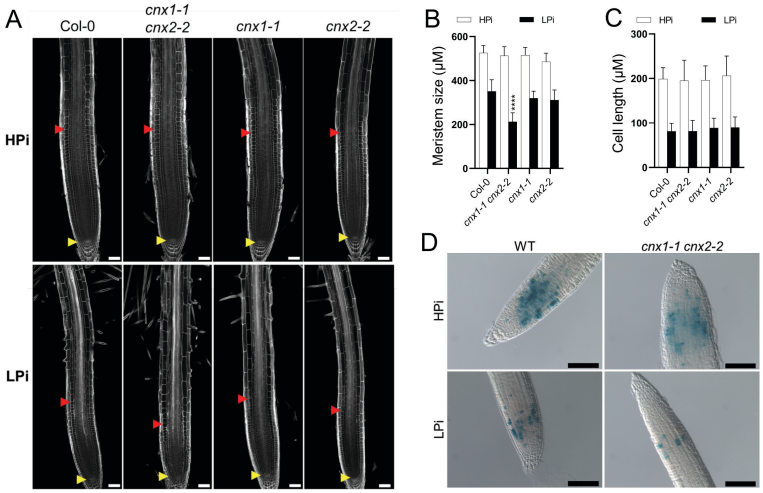

Figure 4. The cnx1-1 cnx2-2 double mutant is affected in meristem activity. (A-C) Plants were grown for 7 days on plates containing HPi or LPi before measuring the length of the cell division zone in the meristem (A, B), defined in A by the yellow and red arrows, and cell length in the differentiation zone (C). Statistical analysis (B, C) was performed by two-way ANOVA followed by a Tukey's test ; significant differences compared to Col-0 under each growth condition are shown: ****, $P < 0.0001$; error bars = SD; $n \geq 5$ in (B) and 20 in (C). (D) Col-0 and cnx1-1 cnx2-2 plants transformed with the cylinB1:GUS reporter gene construct were grown for 7 days on plates containing HPi or LPi medium and stained for β glucuronidase activity. Bars represent 50 um in A and 100 µm in D.

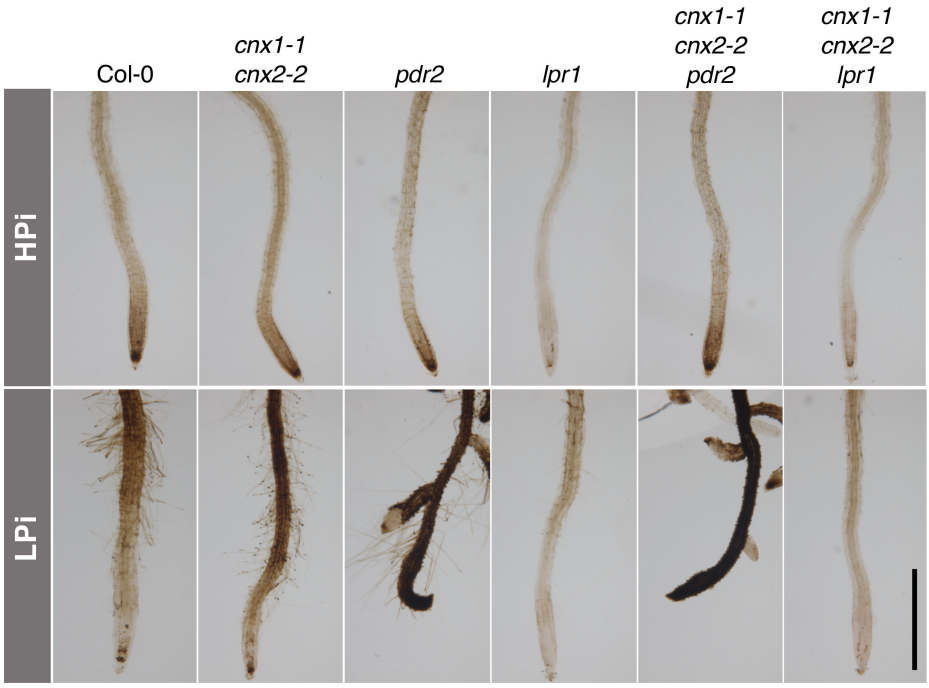

Figure 5. Fe accumulation and distribution in the roots of mutants grown under high and low Pi conditions. Plants were grown for 7 days on plates containing 1 mM or 75 µM Pi and subjected to Perls-DAB staining for Fe visualization. Bar represents 1 mm.

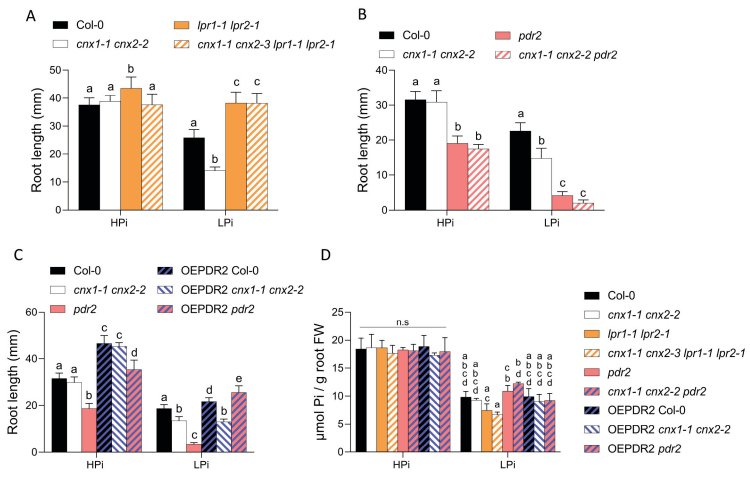

Figure 6. Epistatic interactions among cnx1-1 cnx2-2, lpr1-1 lpr2-1, and pdr2. Plants were grown for 7 days on HPi or LPi plates before recording primary root length. (A) Epistatic interaction between cnx1-1 cnx2-2 and lpr1-1 lpr2-1. (B) Epistatic interaction between cnx1-1 cnx2-2 and pdr2. (C) A T-DNA cassette for PDR2 overexpression under the control of the CaMV35S promoter (OEPDR2) was introgressed into Col-0, cnx1-1 cnx2-2, and pdr2. (D) Pi content in roots for plants grown for 7 days on HPi or LPi. Statistical analysis was performed by two-way ANOVA followed by a Tukey's test, and significant differences within each growth condition are shown. Different lowercase letters (a, b, c, or d) indicate a significant difference with a P-value < 0.05, $n \geq 6$.

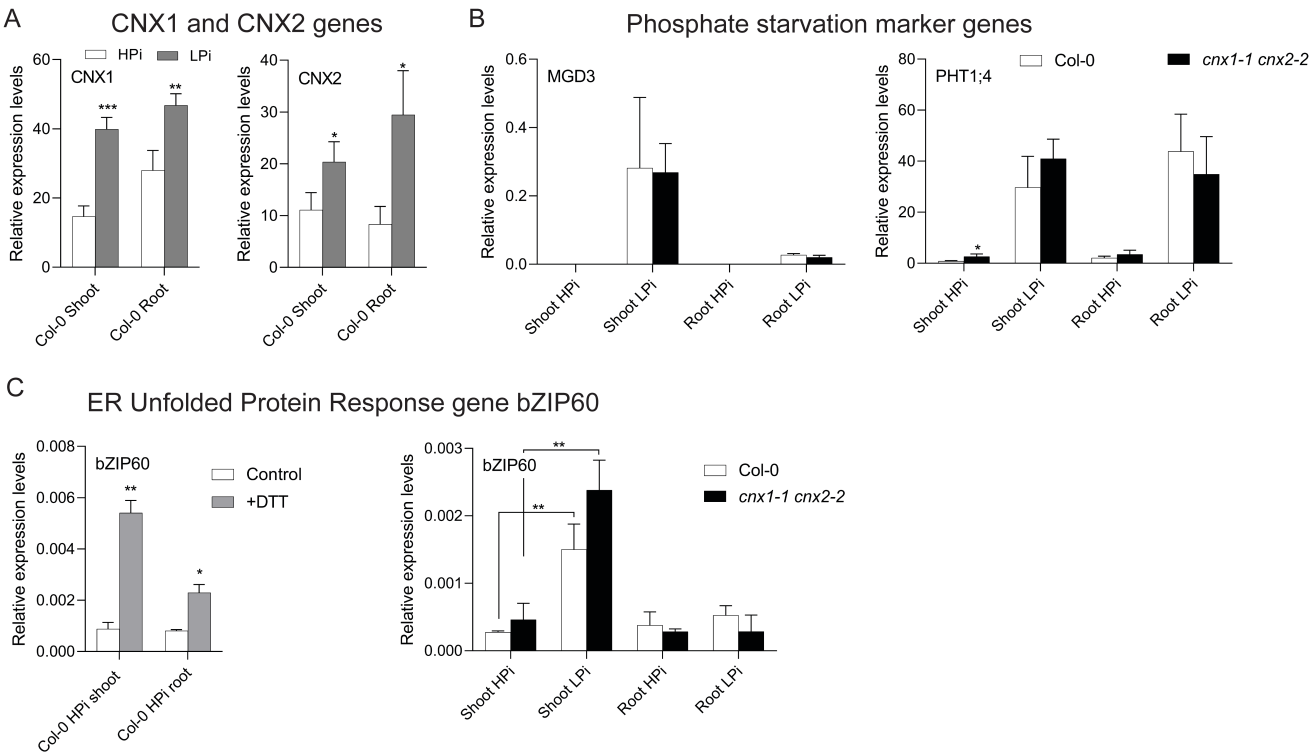

Figure 7. Impact of the *cnx1-1 cnx2-2* mutations on the expression of Pi-deficiency and unfolded protein response marker genes. (A) *CNX1* and *CNX*2 expression in the shoots and roots of plants grown for 7 days in HPi or LPi medium. (B) Expression of the Pi-deficiency markers *MGD3* and *PHT1;4* in the shoots and roots of Col-0 and *cnx1-1 cnx2-2* grown for 7 days on HPi or LPi medium. (C) Induction of ER Unfolded Protein Response marker gene *bZIP60* in the shoots and roots of Col-0 at 24 h after the addition of 2 mM DTT and in the *cnx1-1 cnx2-2* double mutant compared to Col-0 grown under HPi or LPi conditions. Statistical analysis was performed by Student's t test comparing different treatments (HPi and LPi for A and C, Control and DTT for C) and Col-0 vs. *cnx1-1 cnx2-2* (B, C), with significant differences indicated by asterisks (*),*, P <0.05; **, P <0.01; ***, P <0.001. Error bars = SD, n =3.